Hindawi
Advances in Civil Engineering
Volume 2021, Article ID 3668378, 14 pages
https://doi.org/10.1155/2021/3668378

Research Article

Numerical Study on the Influence of Profile Shape on the Stability of a Nonhomogeneous Slope

Guoyu Yang, Tao Shang, Liu Han, and Tao Chen

School of Mines, China University of Mining and Technology, Xuzhou 221116, China

Correspondence should be addressed to Tao Shang; st19621994@163.com

Received 10 August 2021; Revised 22 October 2021; Accepted 23 November 2021; Published 15 December 2021

Academic Editor: Prabhat Kumar Mandal

To study the influence of profile shape on the stability of nonhomogeneous slopes, strip mechanical models of slopes with different profile shapes were established following the simplified Bishop method. Three hundred and seventy slope models with different profile shapes and strata sequences were simulated and analyzed with FLAC3D. The results show that slopes with weaker-to-stronger (WtS) strata sequences are, in most cases, more stable than slopes with stronger-to-weaker (StW) strata sequences when all other conditions are the same. Slopes with linear shapes are the most stable. With increasing arch height, the stability of convex slopes decreases, and the stability of concave slopes first increases slightly and then decreases. When the strata sequences are WtS, the factors of safety (FoSs) of slopes with convex and exterior polyline shapes decrease more slowly. However, when the strata sequences are StW, the FoSs of slopes with concave and interior polyline shapes decrease more slowly. The greatest X-displacements are concentrated in the steeper areas of the slopes. For different strata sequences, the higher the rock strength at the steeper position is, the more stable the slope is, and the opposite trend is also observed. For the same strata sequence, the stability of a polyline-shaped slope is always better than that of a curved slope with the same inflection point.

1. Introduction

In recent years, with the continuous development of open-pit mines, water conservancy projects, road and bridge construction, and other geotechnical engineering projects, the stability of high and steep slopes formed during construction has become increasingly important. Slope stability is a complex geotechnical engineering problem with numerous influencing factors, which can be broadly divided into slope factors (slope height, slope angle, slope shape, geotechnical mechanical properties, etc. [1–4]) and external forces (regional tectonic stress, hydraulic seepage, seismic action, human disturbance, etc. [5–8]). Among these factors, the slope shape is a direct reflection of the geometric characteristics of slopes, and its influence on slope stability has important research significance.

Slope shape can be divided into plan shape and profile shape. Affected by natural action or human disturbance, it often presents convex, concave, and linear shapes [9] (see Figure 1). There are significant differences in slope stability among different slope shapes [10, 11]. A previous force analysis of slopes with different plan shapes showed that under the same other conditions, the direction of the resultant force of the circumferential lateral pressure on the concave slope is opposite to the sliding direction of the slope, while the direction of the resultant force of the circumferential lateral pressure on the convex slope is the same as the sliding direction of the slope [12]. Slope top loading tests have shown that a slope with a concave plan can withstand a greater top peak load, followed by a slope with a linear plan, and a slope with a convex plan can withstand only a small top peak load [13]. In addition, 205 landslide cases that occurred in the Yunyang-Wushan section of the Three Gorges Reservoir area in China after 1970 were statistically analyzed, and it was found that the number of landslides on slopes with concave plans was the lowest, that on slopes with linear plans was the second highest, and that on slopes with convex plans was the highest [14, 15]. In summary, among

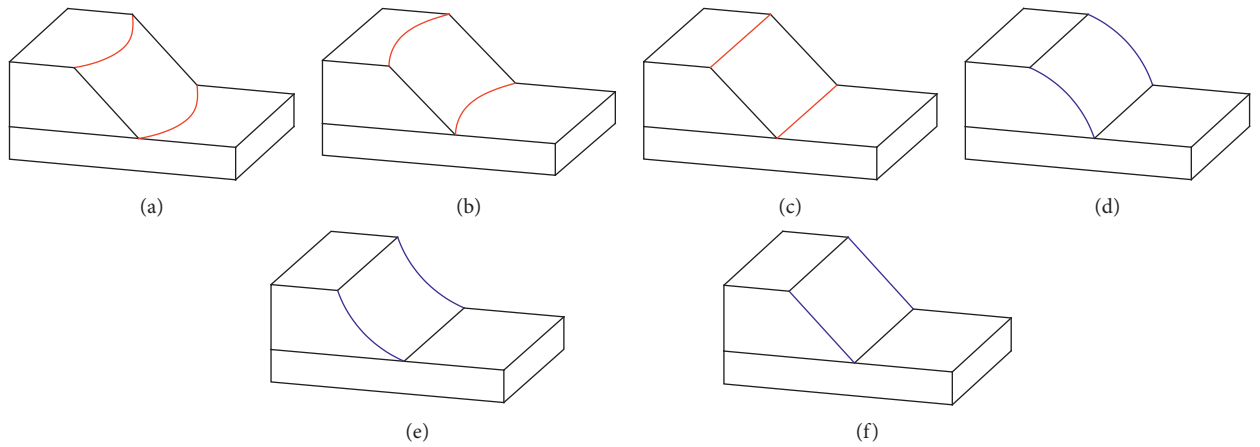

Figure 1: Different slope shapes. (a) Convex plan. (b) Concave plan. (c) Linear plan. (d) Convex profile. (e) Concave profile. (f) Linear profile.

these slope shapes, slopes with concave plans are the most stable, followed by those with linear plans, and the stability of slopes with convex plans is the worst [16, 17].

Different from the plan shape, the profile shape of a slope affects the direction and amount of subsurface flow [18, 19]. Under the conditions of the same rainfall amount and rainfall duration, slopes with concave profiles have a larger volume of fully saturated soil [20], which causes these slopes to be more prone to damage and instability. Moreover, the stability of slopes with different profile shapes was analyzed using the simplified Bishop method and numerical simulation methods. It was found that the stability of slopes with linear shapes was the best, while the stability of slopes with both convex and concave shapes was lower [20, 21].

On the other hand, for the same slope shape, the stability of slopes with different curvatures is also quite different. In general, with the decrease in curvature radius, the stability of slopes with convex plans decreases; in contrast, the stability of slopes with concave plans gradually increases [22]. However, when the curvature radius decreases to a certain extent, the factor of safety (FoS) of the slope will first reach a peak value and then gradually decrease due to the influence of the increasing free surface area of the concave profile slope [23]. In addition, with increasing slope height, the stability enhancement of slopes with concave plans will gradually decrease compared with that of slopes with linear plans [24, 25].

In summary, these studies reveal the influence law of slope shape on slope stability, but their research objects are all homogeneous soil slopes, and no discussion has been provided on how the stability of nonhomogeneous slopes changes with the change in slope shape. There has also been little discussion on the influence of profile shapes with different curvature radii on slope stability. Therefore, this study analyzes the influence of the change in profile shape on the strips in the slope sliding mass based on the simplified Bishop method and reveals the influence law of the profile shape with different curvature radii on the stability of a nonhomogeneous slope using a numerical simulation method.

2. Strip Mechanical Model

The simplified Bishop method is commonly used in engineering to calculate the FoS for circular sliding surfaces [26]. Its calculation model is shown in Figure 2.

Here, r is the radius of the circular sliding surface; α_i and α_j are the base angles of strip i and strip j, respectively; l_i and l_j are the circular lengths of strip i and strip j, respectively; W_i and W_j are the gravities of strip i and strip j, respectively; N_i and N_j are the normal forces of strip i and strip j, respectively; S_i and S_j are the shear resistances of strip i and strip j, respectively; U_i and U_j are the pore water pressures at the bottom of strip i and strip j, respectively; E_i, E_{i+1} and E_j, E_{j+1} are the horizontal interstrip forces of strip i and strip j, respectively; and T_i, T_{i+1} and T_j, T_{j+1} are the vertical interstrip forces of strip i and strip j, respectively.

The simplified Bishop method considers only the force balance in the vertical direction and the overall moment balance and ignores the vertical force between strips. Thus, the FoS of a sliding surface is [27] as follows:

$$\mathrm{FOS} = \frac{\sum_{i=1}^{n} \left[Cl_i \cos\alpha_i + \left(W_i - U_i l_i \cos\alpha_i \right) \tan\varphi \right] 1/\cos\alpha_i + \sin\alpha_i \tan\varphi / \mathrm{FOS}}{\sum_{i=1}^{n} W_i \sin\alpha_i}, \tag{1}$$

where C is the cohesion of the soil and φ is the internal friction angle of the soil.

Equation (1) shows that the FoS is related to l_i, α_i, W_i, U_i, C, and φ. For a certain sliding surface in the slope, C and φ of

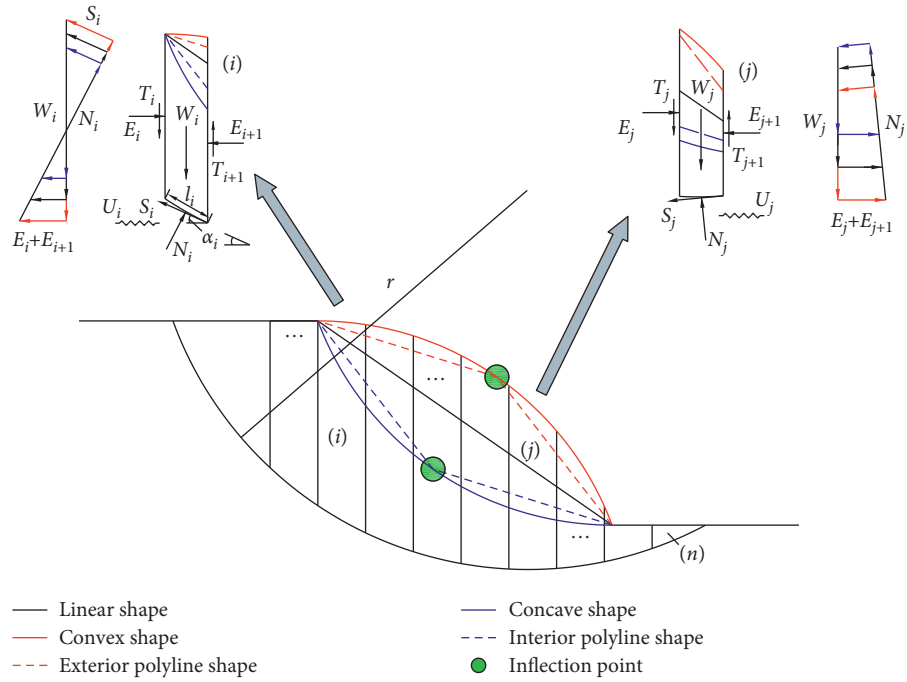

Figure 2: Influence of slope profile shapes on strips.

the soil of the sliding mass are determined to be constant. Therefore, if the method of strip division and the pore water pressure at the bottom of the strips do not change, l_i, α_i, and U_i are also constant, and the FoS of the sliding surface is related only to the gravity of the sliding mass.

As shown in Figure 2, some of the strips in the sliding mass provide a sliding force (such as strip i), which are called sliding strips, while some of the strips provide an antisliding force (such as strip j), which are called antisliding strips. The stress analysis of sliding strip i and antisliding strip j shows that W_i increases when the profile shape changes from a linear shape to a convex shape or exterior polyline shape, and N_i, S_i, and $E_i + E_{i+1}$ are also increased to maintain the balance. When the strip to the right of strip i cannot provide enough horizontal force, strip i will be unstable and slide down. Conversely, when the profile shape changes from a linear shape to a concave shape or interior polyline shape, W_i decreases, and the sliding force produced by strip i decreases.

For the antisliding strip j, when the profile shape changes from a linear shape to a convex shape or exterior polyline shape, W_j increases, but the horizontal force provided by strip j to the strip to the left also increases. In contrast, when the profile shape changes from a linear shape to a concave shape or interior polyline shape, W_j decreases, and the antisliding force provided by strip j also decreases.

Therefore, we can see that the sliding force of the sliding strip and the antisliding force of the antisliding strip are positively related to the gravity of the strip. When the profile shape changes, if the increase in the antisliding force is larger than that of the sliding force or the decrease in the antisliding force is smaller than that of the sliding force, the FoS of the sliding surface will increase; otherwise, the FoS of the sliding surface will decrease.

3. Numerical Simulation Method

The simplified Bishop method requires many iterative calculations to obtain the FoS of each potential sliding surface, and the sliding surface with the smallest FoS is the most critical sliding surface. When the profile shape changes, the most dangerous sliding surface of the slope may also change, so we cannot directly use the simplified Bishop method to compare the magnitudes of change in the sliding force and the antisliding force. The numerical simulation techniques that have become increasingly sophisticated in recent years can not only calculate the FoS of slopes but also simulate the displacement and slippage of slope rock masses. FLAC3D [28] is numerical analysis software that can be used for large-scale geotechnical engineering; it calculates the FoS of slopes by the strength reduction method and has been widely used in the field of slope engineering. In this study, the influence of profile shapes on the stability of nonhomogeneous slopes is numerically simulated using FLAC3D software.

3.1. Curvature Radius of Curved Slopes. The profile shape is controlled by the curvature radius. Taking the concave shape as an example, the value range of the curvature radius is calculated.

Here, α is the slope angle; b is the 1/2 arch span; a_1 is the theoretical maximum arch height; R_1 is the theoretical minimum curvature radius; O_1 is the center of the concave arc with the theoretical minimum curvature radius; D_1 is the vertex of the concave arc with the theoretical minimum curvature radius; a_2 is the actual maximum arch height; R_2 is the actual minimum curvature radius; O_2 is the center of the concave arc with the actual minimum curvature radius; and

D_2 is the vertex of the concave arc with the actual minimum curvature radius.

As shown in Figure 3(a), when $a_1 = b$, the curvature radius of the concave shape can attain the minimum value R_1. At this time, the concave arc lies outside slope lines AB and BC, so the curvature radius of the concave shape cannot take the minimum value R_1. As shown in Figure 3(b), connecting O_1 and D_1 intersects line AC at point N and line BC at point M, and polyline AMC is the constraint boundary of the concave shape. The vertical line of MC intersects the extension line of MN at point O_2. The arc with O_2 as the center and A and C as the endpoints is the limit concave shape of the constraint boundary AMC. R_2 is the minimum value that can be obtained for the curvature radius of the concave shape. Therefore, the curvature radius of the concave shape takes a range of $[b/\sin\alpha, +\infty)$; similarly, the curvature radius of the convex shape takes a range of $[b/\sin\alpha, +\infty)$.

3.2. Model and Material Parameters. To fully study the influence of different profile shapes on slope stability, slope numerical models of different heights and profile shapes are established. These models have heights of 30 m, 60 m, and 90 m, and all have an angle of 45°. The profile shapes of the slope numerical models include a linear shape, a convex arc shape, an exterior polyline shape, a concave shape, and an interior polyline shape. Among them, the inflection point of the exterior polyline shape coincides with that of the convex shape, and the inflection point of the interior polyline shape coincides with that of the concave shape (see Figure 2).

According to the calculation results in Section 3.1, when the slope height is 30 m and the angle is 45°, the curvature radius of both the concave and convex shapes lies in the range [30 m, +∞). When the slope height is 60 m and the angle is 45°, the curvature radius of both the concave and convex shapes lies in the range [60 m, +∞). When the slope height is 90 m and the angle is 45°, the curvature radius of both the concave and convex shapes lies in the range [90 m, +∞). The slope numerical models of different heights are divided into nine curvature classes, as shown in Table 1.

To fully study the influence of the rock strength difference in nonhomogeneous slopes on the stability of slopes with different profile shapes, all of the slope numerical models are divided into three layers. Each layer of a slope with a height of 30 m is 10 m thick, each layer of a slope with a height of 60 m is 20 m thick, and each layer of a slope with a height of 90 m is 30 m thick. The physical and mechanical parameters of the rocks are shown in Table 2.

According to the differences in lithology and the physical and mechanical parameters of the strata, we define a slope with the strata sequence ABC as "weaker to stronger" (WtS) and a slope with the strata sequence CBA as "stronger to weaker" (StW). By comparing the FoSs and displacements of these two types of slopes with different profile shapes, the law governing the influence of profile shape on the stability of nonhomogeneous slopes is explored.

Considering that the inclination and dip angle of the strata may affect the stability of nonhomogeneous slopes with different profile shapes, as the control group, a group of dip slope numerical models with a strata dip angle of 10° and a slope height of 90 m and a group of antidip slope numerical models with a rock strata dip angle of 10° and a slope height of 90 m are added. In total, 370 slope numerical models are constructed in 5 groups. The parameters of the slope numerical models are shown in Table 3.

Considering the calculation accuracy of the numerical models, models with different slope heights have different model sizes and different mesh sizes. When the slope height is 30 m, the dimensions of the slope numerical model are 110 m × 60 m×50 m. Figure 4(a) shows a linear horizontal slope model of 30 m in height with a WtS strata sequence, divided into 32395 grid points and 29100 zones. Other slope numerical models of 30 m in height have similar meshing to this model. When the slope height is 60 m, the dimensions of the slope model are 200 m × 110 m × 100 m. Figure 4(b) shows a concave horizontal slope model of 60 m in height with a StW strata sequence, divided into 27466 grid points and 27593 zones. Other slope numerical models of 60 m in height have similar meshing to this model. When the slope height is 90 m, the dimensions of the slope numerical model are 290 m × 160 m × 150 m. Figure 4(c) shows an interior polyline-shaped horizontal slope model of 90 m in height with a WtS strata sequence, divided into 25522 grid points and 24429 zones. Figure 4(d) shows a convex antidip slope model of 90 m in height with a StW strata sequence, divided into 26685 grid points and 24512 zones. Figure 4(e) shows an exterior polyline-shaped dip slope model of 90 m in height with a WtS strata sequence, divided into 26138 grid points and 23896 zones. Other slope numerical models of 90 m in height have similar meshing to these three models.

4. Results

4.1. FoS. The FoSs of the 5 groups of slope models as calculated by FLAC3D are shown in Figure 5.

As shown in Figure 5, the slopes with WtS strata sequences are, in most cases, more stable than the slopes with StW strata sequences under the same conditions. This indicates that when the weaker strata are located in the lower part of the slope, the slope stability is worse. As the arch height increases, the FoSs of slopes with different profile shapes and different strata sequences generally show a gradually decreasing trend. In particular, with increasing arch height, the FoSs of concave and interior polyline-shaped slopes first increase slightly and then gradually decrease.

The slope numerical models of group *c*, represented in Figure 5(c), are taken as examples for a detailed discussion. When the arch height a is 0, i.e., the profile shape is linear, the FoS of the slope with the WtS strata sequence is 2.164, and the FoS of the slope with the StW strata sequence is 1.707. With a gradual increase in arch height, the FoSs of slopes with different profile shapes and different strata sequences generally show a gradually decreasing trend. When the strata sequence is WtS, as the arch height increases, the FoSs of convex and exterior polyline-shaped slopes decrease more slowly than those

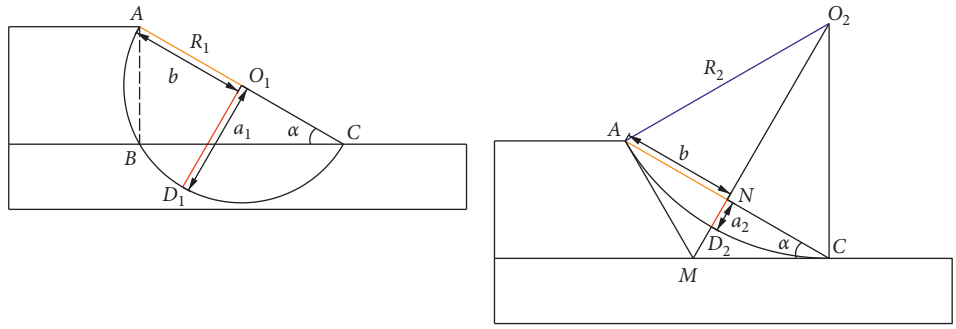

(a) (b)

Figure 3: Calculation diagram of the value range of the arch height and the curvature radius. (a) Theoretical minimum value of curvature radius. (b) Actual minimum value of curvature radius.

Table 1: Curvature classes for slope numerical models.

Slope height (m)	Arch height (m)	Curvature radius (m)	Slope height (m)	Arch height (m)	Curvature radius (m)	Slope height (m)	Arch height (m)	Curvature radius (m)
	1	225.50		2	451.00		3	676.51
	2	113.50		4	227.00		6	640.50
	3	76.50		6	153.00		9	229.50
	4	58.25		8	116.50		12	174.75
30	5	47.50	60	10	95.00	90	15	142.50
	6	40.50		12	81.00		18	121.50
	7	35.64		14	71.29		21	106.93
	8	32.13		16	64.25		24	96.38
	8.79	30.00		17.57	60.00		26.36	90.00

Table 2: Physical and mechanical parameters of the modeled rocks.

Rocks	Bulk modulus (GPa)	Shear modulus (GPa)	Cohesion (kPa)	Internal friction angle(°)	Tensile strength (kPa)	Density (kg/m^3)
Mudstone (A)	6.08	3.47	120	30	96	2460
Silty mudstone (B)	5.12	4.73	216	36	175	2510
Siltstone (C)	10.83	8.13	275	38	220	2460
Sandstone	8.28	6.39	270	33	216	2500

Table 3: Parameters of the slope numerical models.

Group	Slope height/m	Thickness per stratum/m	Inclination/dip angle	Profile shape and strata sequence									
				Linear		Concave		Interior polyline		Convex		Exterior polyline	
				WtS	StW	WtS	StW	WtS	StW	WtS	StW	WtS	StW
a	30	10	Horizontal	1	1	9	9	9	9	9	9	9	9
b	60	20	Horizontal	1	1	9	9	9	9	9	9	9	9
c	90	30	Horizontal	1	1	9	9	9	9	9	9	9	9
d	90	30	Antidip/10°	1	1	9	9	9	9	9	9	9	9
e	90	30	Dip/10°	1	1	9	9	9	9	9	9	9	9

Note. Values of 1 and 9 in the table indicate the numbers of models established in the various cases.

of concave and interior polyline-shaped slopes. When the arch height takes the maximum value of 26.36 m, the FoS of the convex slope (1.715) is 17.71% higher than that of the concave slope (1.457), and the FoS of the exterior polyline-shaped slope (1.816) is 15.37% higher than that of the interior polyline-shaped slope (1.574). In contrast, when the strata sequence is StW, as the arch height increases, the FoSs of concave and interior polyline-shaped slopes decrease more slowly than those of convex and exterior polyline-shaped slopes. When the arch height

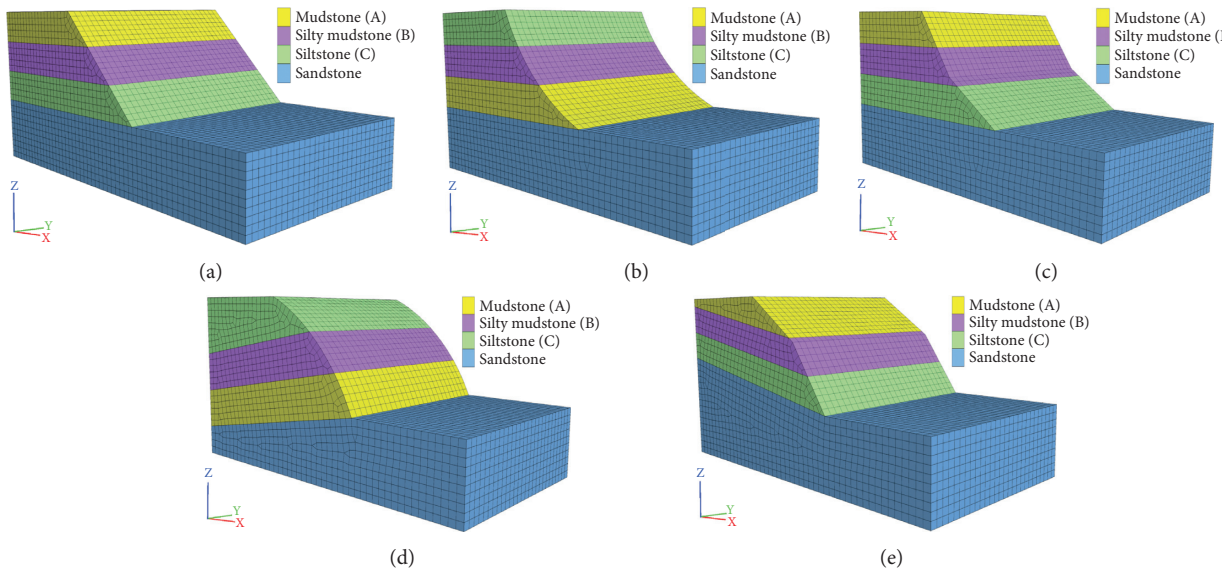

Figure 4: Representative slope numerical models. (a) A linear horizontal slope model of 30 m in height with a WtS strata sequence. (b) A concave horizontal slope model of 60 m in height with an StW strata sequence. (c) An interior polyline-shaped horizontal slope model of 90 m in height with a WtS strata sequence. (d) A convex antidip slope model of 90 m in height with an StW strata sequence. (e) An exterior polyline-shaped dip slope numerical model of 90 m in height with WtS strata sequence.

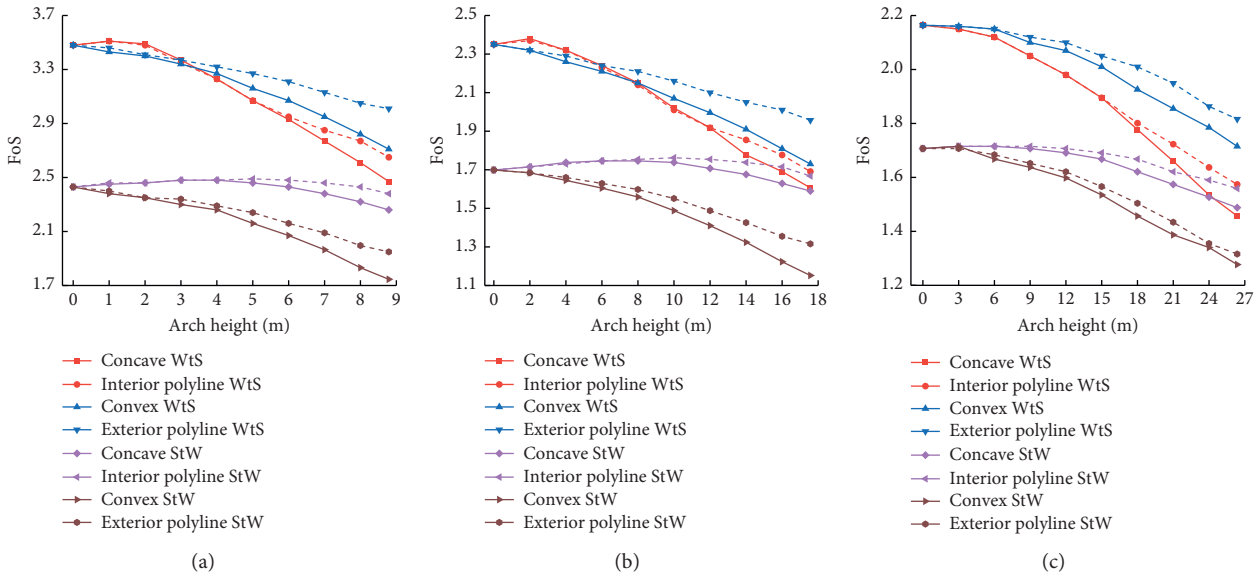

Figure 5: Continued.

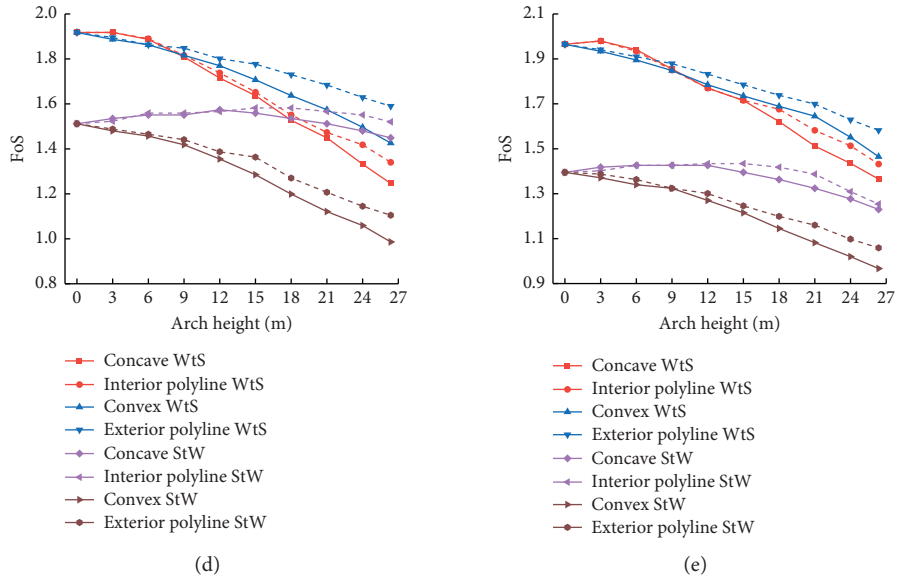

Figure 5: FoSs for slopes with different profile shapes and different strata sequences.

takes the maximum value of 26.36 m, the FoS of the concave slope (1.488) is 16.52% higher than that of the convex slope (1.227), and the FoS of the interior polyline-shaped slope (1.559) is 18.47% higher than that of the exterior polyline-shaped slope (1.316).

When the strata sequence is WtS, the FoSs of concave slopes with arch heights of 3 m and 6 m and interior polyline-shaped slopes with arch heights of 3 m, 6 m, and 9 m are all 1.715, greater than that of a linear slope (1.707).

As seen by comparing Figures 5(a), 5(b), and 5(c), a change in the slope height alters the range of variation in the FoS with the profile shape but does not affect the relative trend of variation in the FoS with the arch height. Similarly, by comparing Figures 5(c), 5(d), and 5(e), it can be found that changes in strata inclination and dip angle affect the FoS variation range, but do not alter the relative variation trend between curves.

In addition, the FoS results of slopes with different profile shapes show that under the same strata sequence conditions, the stability of exterior polyline-shaped slopes is better than that of convex slopes with the same inflection point, and the stability of interior polyline-shaped slopes is better than that of concave slopes with the same inflection point.

4.2. X-Displacement. To investigate the reasons for the difference in the FoS of slopes with different profile shapes under different strata sequences, still taking the slope numerical models of group *c* as examples, X-displacement contour plots of linear slopes, curved slopes with arch heights of 26.36 m, and polyline-shaped slopes with the same inflection point were selected, as shown in Figure 6.

As shown in Figures 6(a) and 6(b), when the strata sequence is WtS, the maximum X-displacement of a linear slope occurs in the upper part of the slope. When the strata sequence is StW, the maximum X-displacement of a linear slope occurs in the lower part of the slope. This means that when the profile shape is linear, the slope is more likely to deform in the weaker rock.

From Figures 6(c), 6(d), 6(e), 6(f), 6(g), 6(h), 6(i), and 6(j), it can be seen that regardless of the strata sequence, the maximum X-displacement of the slopes with a concave shape and interior polyline shape always occurs at the upper part of the inflection point. The maximum X-displacement of the slopes with a convex shape and exterior polyline shape always occurs at the lower part of the inflection point. This reflects that when the profile shape of the slope changes, the slope is more prone to deform in the steeper part.

As shown in Figures 6(c), 6(e), 6(g), and 6(i), for a WtS strata sequence, because slopes with concave and interior polyline shapes are steep at the top and gentle at the bottom, the weak rock above the inflection point is prone to deformation. However, because slopes with convex and exterior polyline shapes are gentle at the top and steep at the bottom, the strong rock below the inflection point is prone to deformation. Because of the different strengths of the strata that are prone to deformation, the FoS differs for the slopes with the same profile shape but different strata sequences.

Additionally, comparing Figure 6(c) and Figure 6(e), the part above the inflection point of the concave slope is steeper than the part above the inflection point of the interior polyline-shaped slope, so the interior polyline-shaped slope is more stable than the concave slope. Similarly, under the condition of the same strata sequence, the stability of the polyline-shaped slope is always better than that of the curved slope with the same inflection point.

5. Discussion

5.1. Comparison with Previous Studies. In this study, a numerical simulation method is used to study the influence of

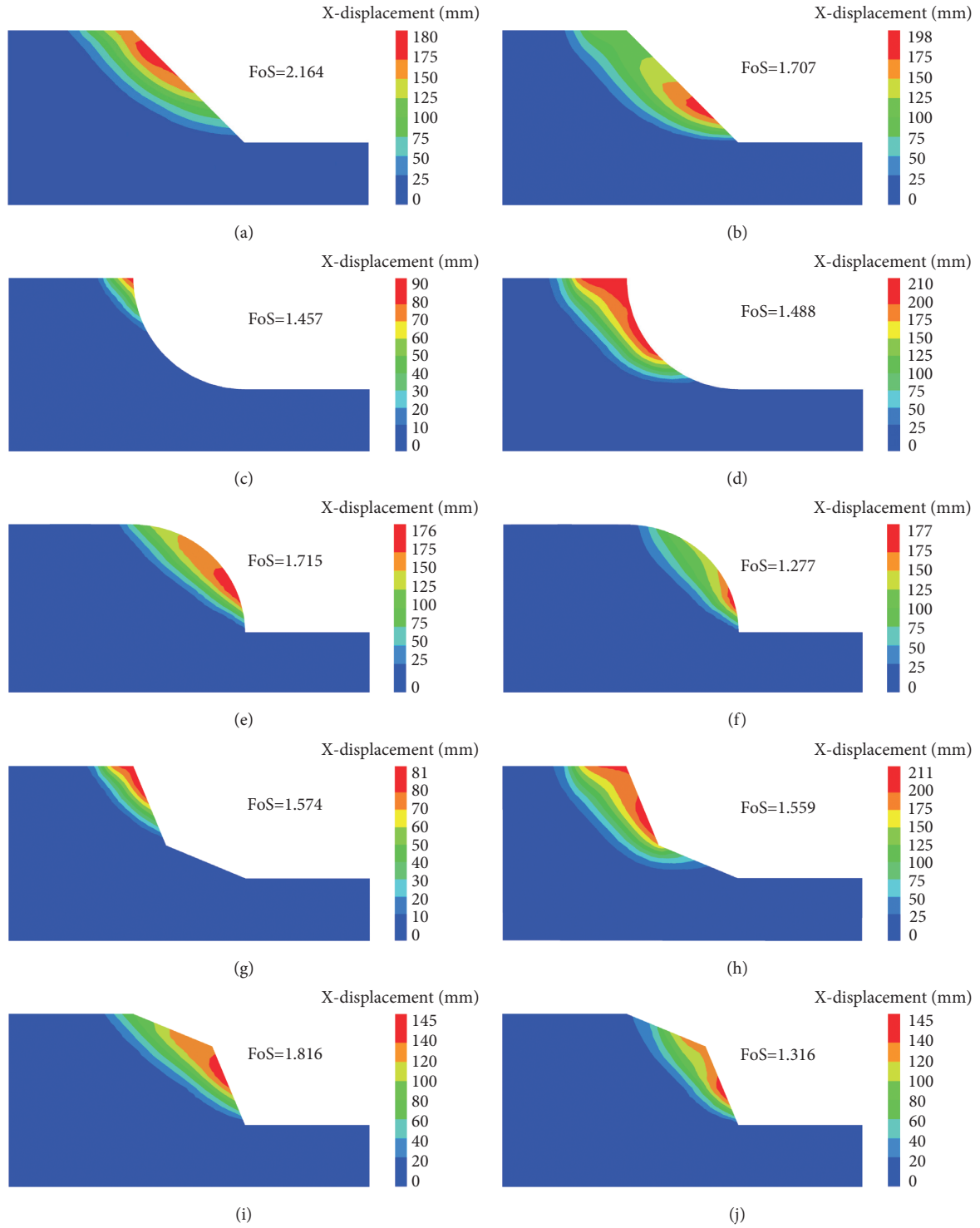

Figure 6: X-displacement contour plots of slopes with different profile slopes and different strata sequences. (a) Linear shape, WtS strata sequence. (b) Linear shape, StW strata sequence. (c) Concave shape, WtS strata sequence. (d) Concave shape, StW strata sequence. (e) Convex shape, WtS strata sequence. (f) Convex shape, StW strata sequence. (g) Interior polyline shape, WtS strata sequence. (h) Interior polyline shape, StW strata sequence. (i) Exterior polyline shape, WtS strata sequence. (j) Exterior polyline shape, StW strata sequence.

different profile shapes on the stability of nonhomogeneous slopes by controlling certain variables. In the past few decades, many studies have considered only the profile shape, one of the many influencing factors of slope stability, for sensitivity analysis. These studies obtained influence laws of profile shape on slope stability by the statistics of numerous landslide cases, but the conclusions are not unified because of the different landslide cases considered in different

studies. For example, F. C. Dai et al. [29] stated that concave slopes have the highest landslide frequency, followed by linear slopes and then convex slopes. A. Shirzadi et al. [2] also proposed that concave slopes have the highest landslide frequency, but W. Chen et al. [3] indicated that convex slopes are more prone to landslides.

In the analysis of single slope cases, more studies have focused on the changes in the stability of slopes with different profile shapes under the action of external factors. To illustrate, profile shape is an important factor in controlling subsurface flow [18]. Under the action of subsurface flow, slopes become unstable more quickly when the profile shape changes from convex to concave [19]. On the other hand, the damage of slopes under seismic action is also closely related to the profile shape [30]. Under the same amplitude, the stability of the slopes with different profile shapes is ordered as follows: from high to low: interior polyline-shaped slope, concave slope, linear slope, exterior polyline-shaped slope, and convex slope [9].

In a similar study, R. H. Sharma [20] also adopted the numerical simulation method, established nine homogeneous slope models with different plan and profile shapes using FLAC3D, and obtained the same conclusion regarding the displacement distribution as identified in this work. That is, the displacement at the top of the concave slope is the largest and that at the bottom of the convex slope is the largest. It is considered that the displacement is caused by the difference in pore water pressure distribution and soil saturation of the slopes with different profile shapes. In contrast, the simulation results obtained in this study under the condition of neglecting the pore water pressure indicate that the maximum displacement occurs at the steeper position in the slope. Nevertheless, the effects of pore water pressure and soil saturation may have exacerbated the displacement performance. In addition, different from this study, these previous studies all take homogeneous slopes as the research object and do not consider the case of non-homogeneous slopes [9, 18, 20, 30]. Moreover, the convex slope and concave slope have fixed curvatures, and the influence of the change in curvature on the slope stability is not discussed.

5.2. Relationship between Inflection Point Positions and Slope Stability. In the analysis of FoS in Section 4.1, we noticed that the FoS of some concave and interior polyline-shaped slopes is slightly higher than that of linear slopes, which may be related to the location of the inflection point. In Section 2, we found that the sliding force of the sliding strip and the antisliding force of the antisliding strip are positively related to the gravity of the strip. Different positions of the inflection point of the slope will change the gravity of the strips. Figure 7 illustrates that compared with the exterior polyline shape corresponding to inflection point 1, the exterior polyline shape corresponding to inflection point 2 increases the gravity of the antisliding strips and reduces the gravity of the sliding strips, which is more beneficial to the slope stability. Similarly, the interior polyline shape corresponding to inflection point 3 decreases the gravity of the sliding strips and increases the gravity of the antisliding strips over those of the interior polyline shape corresponding to inflection point 4, which is more conducive to slope stability. However, this conclusion is still based on the assumption that the most dangerous sliding surface of the slope does not change after the profile shape changes, which needs further discussion and verification.

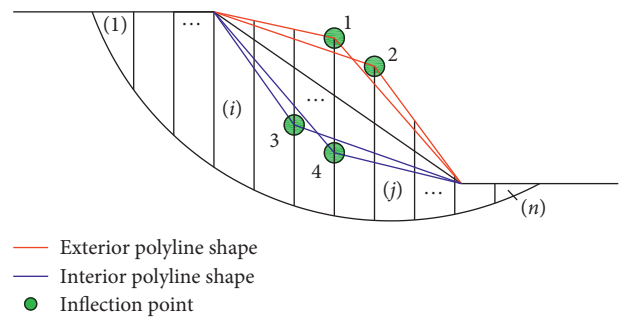

Figure 7: Influence of inflection point positions on strips.

5.3. Engineering Application. The X-displacement simulation results in Section 4.2 show that when the slope shape changes vertically, the slope tends to be destroyed in the steeper part. This phenomenon has important practical significance in the field of engineering technology, especially in the production of open-pit mines. As shown in Figure 8(a), when the coal seam lies at the bottom of the end slope in an open-pit mine, the profile shape of the slope is partially an exterior polyline shape after steep mining. The maximum X-displacement of the slope will occur at the high and steep step below the inflection point. Therefore, if the rock stratum above the coal seam is of high strength, the strength of the overlying rock stratum can be fully utilized to ensure the safety of the slope during mining. After steep mining, the stability of the slope can be improved by simply reinforcing the high and steep steps below the inflection point. Similarly, as shown in Figure 8(b), when the coal seam lies in the middle of the slope, the profile shape of the slope is partially an interior polyline shape after steep mining, while as shown in Figure 8(c), when multiple coal seams exist in the slope, a combination of exterior polyline and interior polyline shapes will be present after steep mining. On the premise that the end slope meets the safety requirements, steep end-slope mining can make full use of the strength of the overlying strata, reduce the stripping ratio, improve the coal recovery rate, and increase the economic benefits.

The north end slope of the Baorixile open-pit coal mine is used as an example to illustrate an engineering application in detail. The Baorixile open-pit coal mine is located in Hulunbuir City, Inner Mongolia Autonomous Region, China. Its geographical location is 118°22′30″–121°10′45″ E and 48°43′18″–50°10′35″ N. The north end slope is 141.46 m high with a slope angle of 22°, and there are three coal seams in the slope, as shown in Figure 9.

A numerical model of the north end slope of the Baorixile open-pit coal mine is established. The model size is 550 m × 300 m×171.46 m. The model is divided into 130474

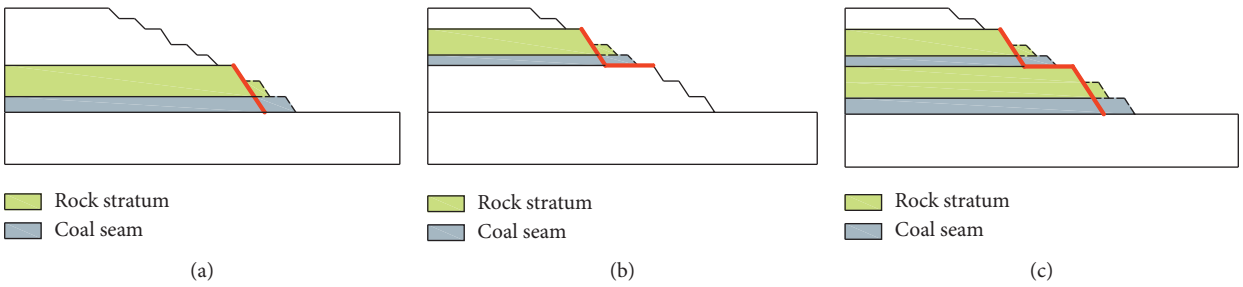

Figure 8: Steep end-slope mining. (a) Coal seam at the bottom of the slope. (b) Coal seam in the middle of the slope. (c) Multiple coal seams in the slope.

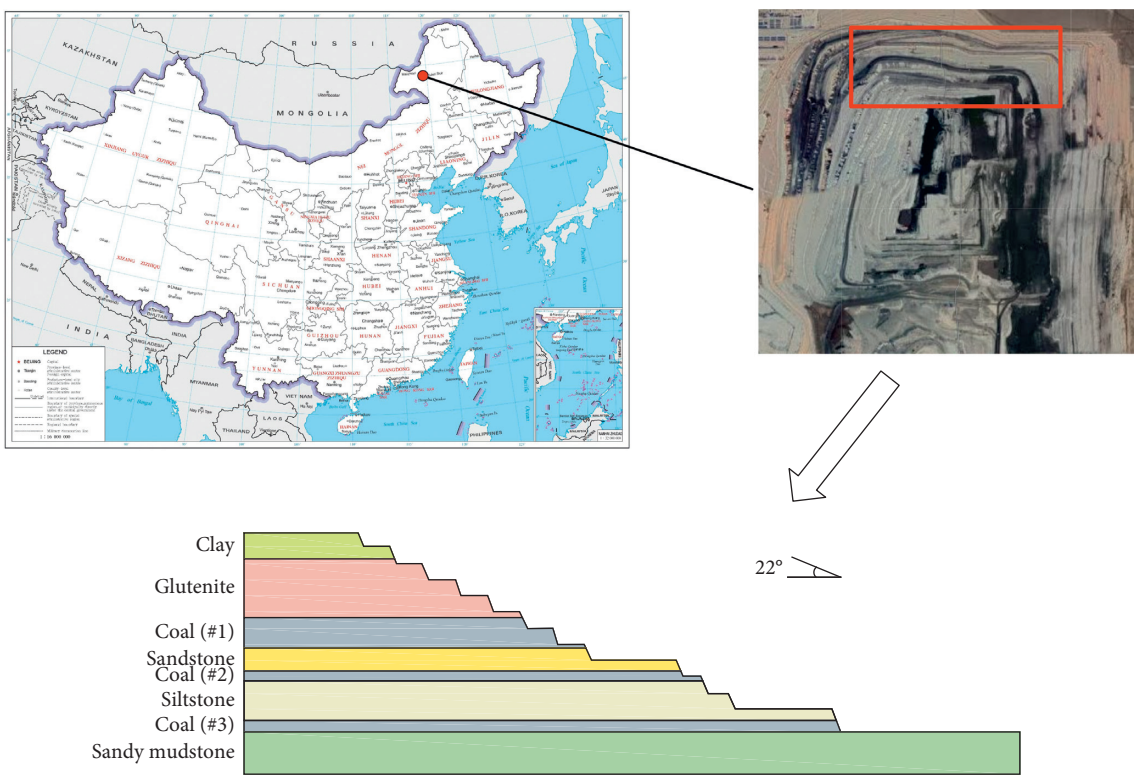

Figure 9: North end slope of the Baorixile open-pit coal mine.

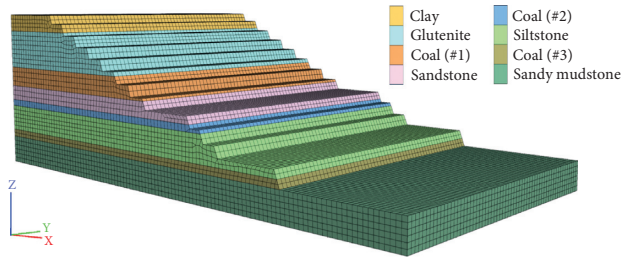

Figure 10: Numerical model of the north end slope of Baorixile open-pit coal mine.

Table 4: Physical and mechanical parameters of the rocks in the north end slope.

Rocks	Thickness/ m	Bulk modulus/ GPa	Shear modulus/ GPa	Cohesion/ kPa	Internal friction angle/°	Tensile strength/ kPa	Density/ kg/m^3
Clay	18.46	0.28	0.093	42	25	40	1960
Glutenite	41.75	5.10	3.30	112	37	90	2650
Coal (#1)	21.62	4.91	2.01	65	32	52	1380
Sandstone	16.34	5.97	6.01	103	40	72	2480
Coal (#2)	21.62	4.91	2.01	65	32	52	1380
Siltstone	28.16	5.00	3.80	127	35	101	2500
Coal (#3)	21.62	4.91	2.01	65	32	52	1380
Sandy mudstone	30.00	4.90	3.20	58	35	46	2520

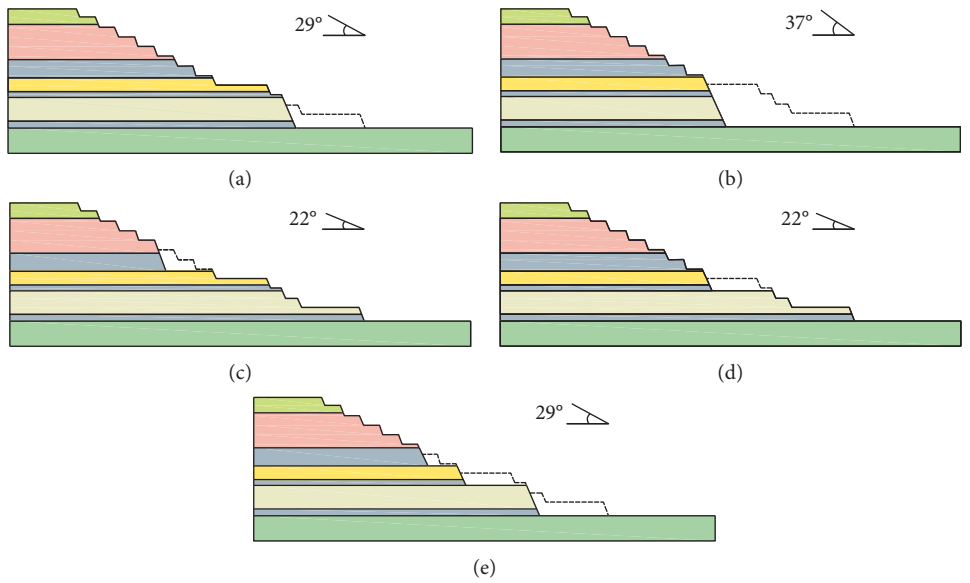

Figure 11: Steep end-slope mining schemes. (a) Scheme I merges the bottom 3 steps. (b) Scheme II merges the bottom 5 steps. (c) Scheme III merges the upper-middle 3 steps. (d) Scheme IV merges the lower-middle 3 steps. (e) Scheme V merges 7 steps in different positions.

grid points and 124098 zones, as shown in Figure 10. The physical and mechanical parameters of the rocks in the north end slope are shown in Table 4.

Based on the locations of the coal seams in the north end slope, 5 schemes are proposed for steep end-slope mining: in Scheme I, the bottom 3 steps are merged; in Scheme II, the bottom 5 steps are merged; in Scheme III, the upper-middle 3 steps are merged; in Scheme IV, the lower-middle 3 steps are merged; and in Scheme V, 7 steps in different positions are merged, as shown in Figure 11.

In the excavation simulations carried out using the FLAC3D software, the simulated excavation sequences proceed step by step from top to bottom for all schemes. The FoSs and X-displacement contour plots of the initial north end slope and the slopes after steep mining under each scheme are shown in Figure 12.

As shown in Figure 11, compared with the initial north end slope, the FoS of the slope after steep end-slope mining decreases under each scheme, but it is still greater than 1, meeting the slope safety requirements. From Figure 12(a), it can be seen that the maximum X-displacement of the initial north end slope occurs at the top of the #1 coal seam step because the #1 coal seam is weaker and 21.62 m thick. Figures 12(b) and 12(c) show that when the bottom steps are merged, the profile shape of the slope is partially an exterior polyline shape, so the maximum X-displacement occurs at the steepest position of the slope below the inflection point. Figures 12(d) and 12(e) show that when the middle steps are merged, the profile shape of the slope is partially an interior polyline shape, so the maximum X-displacement occurs at the steepest position of the slope above the inflection point. For the scheme of merging 7 steps in different positions, as shown in Figure 11(e), we can clearly observe that three high and steep steps are formed on the slope after steep end-slope mining. Among these high and steep steps, the height (36.33 m) and angle (67°) of the step at the bottom are greater than those of the middle step (23.3 m in height and 66° in angle) and the upper step (21.62 m in height and 64° in angle), so the maximum X-displacement of the slope occurs at the bottom high and steep step. After steep end-slope

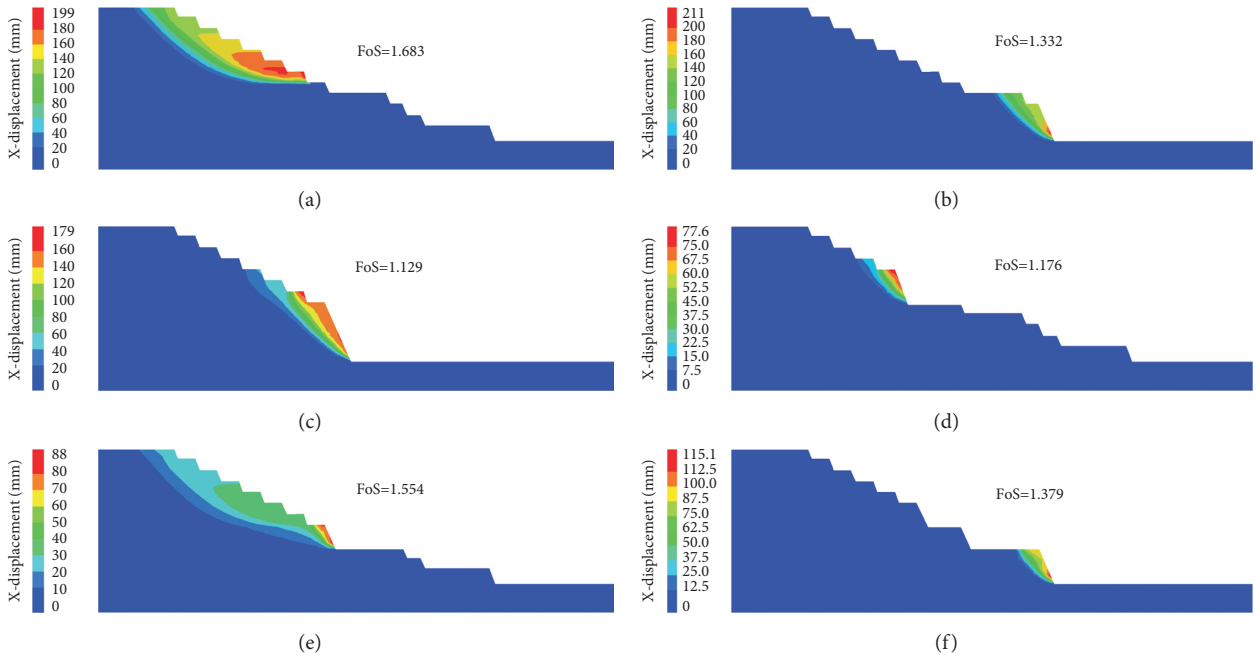

FIGURE 12: FoSs and X-displacement contour plots of the initial slope and the slope after steep mining under the different schemes. (a) Initial north end slope. (b) Scheme I. (c) Scheme II. (d) Scheme III. (e) Scheme IV. (f) Scheme V.

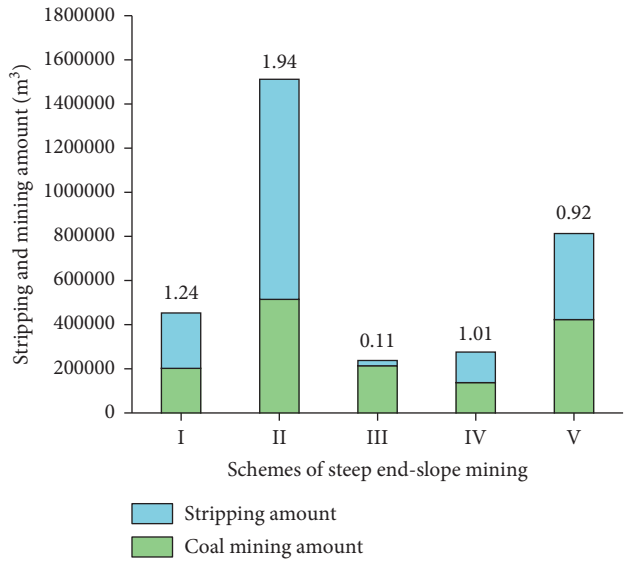

FIGURE 13: Mining and stripping amounts and stripping ratio for each steep end-slope mining scheme.

mining, the slope stability can be improved by reinforcing the high and steep steps that are prone to displacement in each scheme.

Based on the recoverable length of 300 m, the mining and stripping amounts and the stripping ratio for each steep end-slope mining scheme are shown in Figure 13. Each of the steep end-slope mining schemes can increase coal recovery at a very low strip ratio.

6. Conclusions

In this study, a strip mechanical model of slopes with different profile shapes was established based on the simplified Bishop method. Three hundred and seventy slope numerical models with different profile shapes and different strata sequences were constructed, and the influence of profile shape on the stability of nonhomogeneous slopes was studied using FLAC3D software. The conclusions are as follows:

(1) The sliding force of the sliding strip and the antisliding force of the antisliding strip are positively related to the gravity of the strips. The gravity of the strips will change with the profile shape of the slope.

(2) Under otherwise identical conditions, a slope with a WtS strata sequence is more stable than that with an StW strata sequence.

(3) The stability of a linear slope is the best among the slope shapes investigated. With increasing arch height, the stability of a convex slope decreases, and the stability of a concave slope first increases slightly and then decreases. When the strata sequence is WtS, convex and exterior polyline-shaped slopes are more stable, while when the strata sequence is StW, concave and interior polyline-shaped slopes are more stable. The height of the slope and the inclination and dip angle of the strata do not affect the trend of variation of the FoS.

(4) When the profile shape of a slope changes, the slope is more prone to deform in the steeper part. For different strata sequences, the higher the rock strength at the steeper position is, the more stable the slope is, and the lower the rock strength is, the more unstable the slope is. For the same strata sequence, the stability of a polyline-shaped slope is always better than that of a curved slope with the same inflection point.

Data Availability

The data used to support the findings of this study are included within the article.

Conflicts of Interest

The authors declare that there are no conflicts of interest regarding the publication of this study.

Acknowledgments

This research was funded by the National Key Research and Development Program of China (2016YFC0501103) and the National Natural Science Foundation of China (51804298 and 51774271).

References

[1] G. C. Ohlmacher, "Plan curvature and landslide probability in regions dominated by earth flows and earth slides," *Engineering Geology*, vol. 91, no. 2–4, pp. 117–134, 2007.

[2] A. Shirzadi, D. T. Bui, B. T. Pham et al., "Shallow landslide susceptibility assessment using a novel hybrid intelligence approach," *Environmental Earth Sciences*, vol. 76, no. 2, 2017.

[3] W. ChenM. Panahi et al., "Applying population-based evolutionary algorithms and a neuro-fuzzy system for modeling landslide susceptibility," *Catena*, vol. 172, pp. 212–231, 2019.

[4] D. Park and R. L. Michalowski, "Three-dimensional stability analysis of slopes in hard soil/soft rock with tensile strength cut-off," *Engineering Geology*, vol. 229, pp. 73–84, 2017.

[5] I. Baroň, L. Sokol, R. Melichar, and L. Plan, "Gravitational and tectonic stress states within a deep-seated gravitational slope deformation near the seismogenic Periadriatic Line fault," *Engineering Geology*, vol. 261, Article ID 105284, 2019.

[6] S. Peruccacci, M. T. Brunetti, S. L. Gariano, M. Melillo, M. Rossi, and F. Guzzetti, "Rainfall thresholds for possible landslide occurrence in Italy," *Geomorphology*, vol. 290, pp. 39–57, 2017.

[7] H. Tanyas, M. Rossi, M. Alvioli, C. J. V. Westen, and I. Marchesini, "A global slope unit-based method for the near real-time prediction of earthquake-induced landslides," *Geomorphology*, vol. 290, pp. 39–57, 2019.

[8] C. Zhu, M. He, M. Karakus, X. Cui, and Z. Tao, "Investigating toppling failure mechanism of anti-dip layered slope due to excavation by physical modelling," *Rock Mechanics and Rock Engineering*, vol. 53, no. 11, pp. 5029–5050, 2020.

[9] Z. P. Zhang, C. Y. Chang, and Z. Y. Zhao, "Influence of the slope shape on seismic stability of a slope," *Advances in Civil Engineering*, vol. 2020, Article ID 8827072, 8 pages, 2020.

[10] T. K. Nian, R. Q. Huang, S. S. Wan, and G. Q. Chen, "Three-dimensional strength-reduction finite element analysis of slopes: geometric effects," *Canadian Geotechnical Journal*, vol. 49, no. 5, pp. 547–588, 2012.

[11] Y. Zhang, G. Chen, L. Zheng, Y. Li, and X. Zhuang, "Effects of geometries on three-dimensional slope stability," *Canadian Geotechnical Journal*, vol. 50, no. 3, pp. 233–249, 2013.

[12] K. L. Lu and D. Y. Zhu, "Theoretical and experimental study of effect of slope topography on its stability," *Chinese Journal of Rock Mechanics and Engineering*, vol. 33, no. 1, pp. 35–42, 2014.

[13] X. J. Fang and J. H. Wang, "Model tests study on effect of slope geometry and water content on three-dimensional slope failure of sandy slope," *Science Technology and Engineering*, vol. 18, no. 19, pp. 113–119, 2018.

[14] C. Y. Wu, J. P. Qiao, and L. B. Lan, "Research on slope shape of landslide based on gis technique," *Journal of Natural Disasters*, vol. 14, no. 3, pp. 34–37, 2005.

[15] J. P. Qiao, C. Y. Wu, and H. L. Tian, "Contributing ratios of the slope shape toward the landslide development from Yunyang to Wushan in three gorges reservoir area," *Journal of Engineering Geology*, vol. 14, no. 1, pp. 18–22, 2006.

[16] C. W. Sun, J. R. Chai, Z. G. Xu, and Y. Qin, "3D stability charts for convex and concave slopes in plan view with

homogeneous soil based on the strength-reduction method," *International Journal of Geomechanics*, vol. 17, no. 5, Article ID 06016034, 2017.

[17] D. P. Deng, L. Li, and L. H. Zhao, "Method of generation and model of calculation of arbitrary curved slip surfaces for three-dimensional convex and concave slopes," *International Journal of Geomechanics*, vol. 17, no. 11, Article ID 04017095, 2017.

[18] A. G. J. Hilberts, E. E. V. Loon, P. A. Troch, and C. Paniconi, "The hillslope-storage Boussinesq model for non-constant bedrock slope," *Journal of Hydrology*, vol. 291, no. 3-4, pp. 160–173, 2004.

[19] A. Talebi, R. Uijlenhoet, and P. A. Troch, "A low-dimensional physically based model of hydrologic control of shallow landsliding on complex hillslopes," *Earth Surface Processes and Landforms*, vol. 33, no. 13, pp. 1964–1976, 2008.

[20] R. H. Sharma, "Evaluating the effect of slope curvature on slope stability by a numerical analysis," *Australian Journal of Earth Sciences*, vol. 60, no. 2, pp. 283–290, 2013.

[21] K. Cha and T. Kim, "Evaluation of slope stability with topography and slope stability analysis method," *KSCE Journal of Civil Engineering*, vol. 15, no. 2, pp. 251–256, 2011.

[22] Y. M. Cheng, H. T. Liu, W. B. Wei, and S. K. Au, "Location of critical three-dimensional non-spherical failure surface by NURBS functions and ellipsoid with applications to highway slopes," *Computers and Geotechnics*, vol. 32, no. 6, pp. 387–399, 2005.

[23] L. Han, J. S. Shu, W. Zhou, and Q. W. Meng, "Research on mechanical and geometric characteristics of concave end-slope in open-pit mine with mining by areas," *Journal of Huazhong University of Science and Technology (Nature Science Edition)*, vol. 42, no. 3, pp. 82–86, 2014.

[24] L. Ma, K. M. Li, L. Han, J. S. Shu, and Q. W. Meng, "Comparative study on stability and mechanical structure of straight slope and horizontal concave slope," *Journal of Mining & Safety Engineering*, vol. 33, no. 4, pp. 729–733, 2016.

[25] T. Zhang, Q. Cai, L. Han, J. Shu, and W. Zhou, "3D stability analysis method of concave slope based on the Bishop method," *International Journal of Mining Science and Technology*, vol. 27, no. 2, pp. 365–370, 2017.

[26] D. Y. Zhu, J. H. Deng, and J. J. Tai, "Theoretical verification of rigorous nature of simplified Bishop method," *Chinese Journal of Rock Mechanics and Engineering*, vol. 26, no. 3, pp. 455–458, 2007.

[27] A. W. Bishop, "The use of the slip circle in the stability analysis of slopes," *Géotechnique*, vol. 5, no. 1, pp. 7–17, 1955.

[28] Itasca, *FLAC3D (Fast Lagrangian Analysis of Continua in 3 Dimensions)*, Itasca Consulting Group, Minneapolis, MN, 2012.

[29] F. C. Dai and C. F. Lee, "Landslide characteristics and slope instability modeling using GIS, Lantau Island, Hong Kong," *Geomorphology*, vol. 42, no. 3-4, pp. 213–228, 2002.

[30] Z. X. Yan, S. Shi, B. Dang, and B. Li, "Influence of the slope shape on the stability of rock slope under the seismic," *Journal of Shandong University of Science and Technology*, vol. 32, no. 2, pp. 43–48, 2013.